Electrical properties of BaTiO3 based ferroelectric capacitors grown on oxide sacrificial layers for micro-cantilevers applications

Vasta, Giuseppe; Jackson, Timothy; Tarte, Edward

DOI:
10.1016/j.tsf.2011.11.032

G. Vasta, T. J. Jackson, E. Tarte

Electrical properties of BaTiO3 based ferroelectric capacitors grown on oxide sacrificial layers for microcantilevers applications

Thin Solid Films
520 (2012) 3071–3078

DOI: 10.1016/j.tsf.2011.11.032

Electrical properties of $BaTiO_3$ based ferroelectric capacitors grown on oxide sacrificial layers for micro-cantilevers applications

Giuseppe Vasta [a], Timothy J. Jackson [b], Edward Tarte [c]

The University of Birmingham, School of Electrical Electronic and Computer Engineering, 52 Pritchatts road, Edgbaston, Birmingham B15 2TT UK

[a] email: pipvast@yahoo.it; tel: (+44) (0)1214144348 (corresponding author)

[b] email:T.J.Jackson@bham.ac.uk; tel: (+44) (0)121414 4291

[c] email: tartee@adf.bham.ac.uk; tel: (+44) (0)121414 4301

Abstract:

An investigation of all oxides ferroelectric capacitors based on $SrRuO_3/BaTiO_3/SrRuO_3$ multi-layers grown on sacrificial oxide layers of $YBa_2Cu_3O_7$ and MgO for Micro-Electo-Mechanical systems applications is reported. By insertion of additional MgO or $SrTiO_3$ buffer layers the orientation of the $BaTiO_3$ film can be controlled allowing the fabrication of suspended cantilevers using the 31 and the 33 piezoelectric modes. The electrical properties of $SrRuO_3/BaTiO_3/SrRuO_3$ capacitors are changed compared with those grown directly on a single crystal substrate by the introduction of sacrificial layers. Circuit modeling of the electrical

characteristics of these devices shows that a reduction of the deposition pressure for $BaTiO_3$ produces a decrease of the parasitic shunting conductance (modeled with a resistor in parallel to the capacitance of the device) which reduces the resistive loss present in the $BaTiO_3$ film. However for extremely low deposition pressure the quality of the polarization hysteresis loops is compromised.

Particulates present on the surface of the $YBa_2Cu_3O_7$ increases the parasitic conductance at low frequency in the capacitive structure grown on this sacrificial layer. Good electrical properties are obtained for the capacitive structures grown on top of the MgO sacrificial layers at pressures equal or lower than 8 Pa.

Keywords: $BaTiO_3$ ferroelectric capacitor; impedance measurement; ,$YBa_2Cu_3O_7$ and MgO sacrificial layer;, piezoelectric cantilevers.

1 Introduction

In recent years investigations of piezoelectric materials with a perovskite structure and containing lead, have been widely performed for applications such as Micro-Electro-Mechanical systems (MEMS) energy harvesting devices [1,2] or sensors and actuators [3,4,5,6]. Lead containing piezoelectric-perovskite materials provide high strain-charge displacement conversion, but the environmental problems associated with lead have stimulated recent work focusing on the use of lead free piezoelectric materials [7].

$BaTiO_3$ is a lead free piezoelectric material whose growth has been investigated on a range of substrates [8,9,10,11]. A number of studies have reported the performance of $BaTiO_3$ based ferroelectric capacitors [12] which can find applications also in the field of memories [6]. This work focuses on the properties of $BaTiO_3$ thin films in MEMS device like micro-cantilevers with a view to applications as sensors, actuators and energy harvesting devices. Sacrificial layers on which a multi-layer stack can be grown are necessary to fabricate micro-cantilevers. The properties of $BaTiO_3$ capacitors grown on different multi-layers are expected to differ from the properties of the thin films directly deposited on the substrate.

We have recently shown that it is possible to suspend multilayer cantilevers containing a $BaTiO_3$ film grown on $YBa_2Cu_3O_7$ sacrificial layers [7]. The advantage of using $YBa_2Cu_3O_7$ as sacrificial layer is the ease with which it can be etched in weak HNO_3 solutions. In addition its perovskite-based structure allows the growth on its surface of epitaxial multi-layers of $SrRuO_3/BaTiO_3/SrRuO_3$ and $SrRuO_3/BaTiO_3/SrRuO_3/SrTiO_3$ which can be used as a 31 mode energy harvester, or $SrRuO_3/BaTiO_3/MgO/SrTiO_3$ which can be used as a 33 mode energy harvester [7]. In our previous work [7], the electrical properties of these capacitive structures grown on a (001) oriented $SrTiO_3$ substrate were reported. However as we will show, when these capacitors are grown on thick (over 400 nm) $YBa_2Cu_3O_7$ or MgO sacrificial layers the electrical properties of the $BaTiO_3$ change. This article describes the results of a study of the electrical properties of these structures as function of the deposition conditions.

2 Experimental procedure

Multi-layer thin films were grown on **(001)** oriented $SrTiO_3$ substrates by Pulsed Laser Deposition using a KrF excimer laser with a wavelength of 248 nm. A 4 Hz repetition rate was used with the laser beam focused to a spot size of 2.4 mm^2 on the target providing a fluence of 3.4 J/cm^2. The distance between the $SrTiO_3$ substrate and the target material was set to 5.7 cm. All the films were grown in an oxygen flow environment at pressures of 20 Pa for the $YBa_2Cu_3O_7$, 40 Pa for the $SrRuO_3$, 26.66 Pa for the MgO, 8 Pa, 0.40 Pa and 0.013 Pa for the $BaTiO_3$ and 28 Pa for the $SrTiO_3$.

The $YBa_2Cu_3O_7$ film were deposited at a temperature of 740 °C in order to reduce the number of outgrowths which usually form at higher deposition temperatures [13], all the other layers were grown at the temperature of 780 °C. After the deposition, the multi-layers were cooled in 900 mbar O_2 static environment, with dwells of 15 minutes at 600 °C and of 30 minutes at 450 °C during cooling to fully oxygenate the $YBa_2Cu_3O_7$ layer [14]. The dwells were maintained also in the case of stacks of thin films which did not contain the $Ya_2Cu_3O_7$ in order to maintain consistency for oxygenation of the $BaTiO_3$ layer [8]. Compared to the other oxide films, the $BaTiO_3$ was grown to a relatively low pressure.

The thin films were patterned by contact photolithography and argon ion beam milling, using a Karl Suss mask aligner and an Oxford Applied Research IM150 ion milling system. Photoresist was used to protect the regions of the sample which would become the cantilevers. Milling through windows developed in the photoresist, was used to define the cantilever geometry. The cantilevers were released by undercutting the sacrificial layer in HNO_3 solutions. A concentration of 0.1% was used to undercut the $YBa_2Cu_3O_7$ sacrificial layer while a concentration of 20% was needed to undercut the MgO sacrificial layer. The sample was then

rinsed in distilled water and dried by using critical point drying in order to avoid the breakage of the suspended structures due to stiction [15].

In the case of the 31 piezoelectric capacitors, the $YBa_2Cu_3O_7$ or the MgO sacrificial layer together with a thin $SrTiO_3$ film and a $SrRuO_3$ conductive layer were grown first and then the bottom electrodes and their contact pads were patterned by contact photolithography and argon ion beam milling. The sample was then returned to the deposition chamber, 15 minutes of annealing at the $BaTiO_3$ deposition temperature was performed, to repair the regions damaged by the milling, followed by deposition of the $BaTiO_3$ piezoelectric film and the $SrRuO_3$ film. Finally the top electrode was patterned and some windows, necessary to contact the bottom electrode layer, were opened through the $BaTiO_3$.

In the case of the 33 piezoelectric capacitors the $YBa_2Cu_3O_7$ sacrificial layer was first grown followed by the deposition of a $SrTiO_3$ and of a MgO thin film. The vacuum was then broken (our deposition system allows the deposition in situ of only three films) and then another thin MgO layer, the $BaTiO_3$ and the $SrRuO_3$ were deposited. Finally the top electrodes and their contact pads were patterned. In the case of an MgO sacrificial layer, the MgO, the $BaTiO_3$ and the $SrRuO_3$ can be grown in situ and then the top electrode can be patterned.

Atomic Force Microscope (AFM) measurements on the surface of the deposited film were performed in contact mode on an area of 10 μm x 10 μm at a frequency of 0.4 Hz. The measurements system consists of a Veeco autoprobe CB based unit AP0100 controlled by a data acquisition software supplied by Veeco.

The structure of the films was assessed by using X-ray diffraction. The measurements were performed using the $CuK\alpha_1$ radiation (1.54056 Å) of a four circle Siemens D5000 diffractometer, the symmetrical Bragg-Brentano configuration has been used**.**

The diffractometer software allows the angles at which diffraction peaks are expected to be determined. The detector is then moved to the indicated positions and a scan is run. If the diffraction peak is found in the indicated position, further scans allow a refinement in the evaluation of the diffraction angle.

Capacitance measurements were performed on both the 31 and the 33 structures by means of an Agilent 4294A precision impedance analyzer with a source voltage of 1 V over the frequency range of 50 Hz – 50 kHz.

Hysteresis loop measurements were run on the 31 structures by using a custom made Sawyer and Tower circuit and applying sinewave voltages with peak to peak amplitude up to 50 V and frequency of 20 kHz.

3 Device description and modeling

The scope of this article is the investigation of multi-layer cantilevers, containing a $BaTiO_3$ based capacitive structure for use as energy harvesting devices. These devices convert the mechanical vibrations of suspended beams, which may be terminated with a proof mass, into an electrical signal, which may be used as a source of electrical power.

There are two piezoelectric modes which are commonly used in piezoelectric transducers, they are the 33 and the 31 modes, fig 1 [1,2]. In a 31 mode device the input stress σ_{xx} is perpendicular

to the developed electric field and the mechanical strain is converted into the separation of charge by using a parallel plate capacitor.

In a 33 mode device the input stress σ_{xx} is parallel to the developed electric field and the mechanical strain is converted into charges by using an interdigitated capacitor.

The generated output voltage can be expressed as [1,2]:

$$V_{3i} = \sigma_{xx}\, g_{3i}\, t \qquad (1)$$

where g_{3i} [Vm/N] is the piezoelectric constant, and t is the electrode spacing. The output voltage is expected to be larger in the 33 mode because the $BaTiO_3$ piezoelectric constant g_{33} is larger than the g_{31} piezoelectric constant [16], furthermore the electrode spacing is bigger in the 33 mode.

In our case the 31 mode devices are given by the following layer sequences:

$SrRuO_3/BaTiO_3/SrRuO_3$ and $SrRuO_3/BaTiO_3/SrRuO_3/SrTiO_3$ grown on a MgO or on a $YBa_2Cu_3O_7$ sacrificial layer respectively. For the 33 mode devices the stack $SrRuO_3/BaTiO_3/MgO/SrTiO_3$ can be grown on a $YBa_2Cu_3O_7$ sacrificial layer, alternatively a $SrRuO_3/BaTiO_3$ bi-layer can be grown on a MgO sacrificial layer. The reason for the choice of such layer sequences will be explained in the subsection 4.1.

The model which has been adopted to describe the fabricated capacitors is that one depicted in fig. 2 where C represents the capacitance of the device, R is a parallel resistor modeling the parasitic shunting conductance representing the losses present in the $BaTiO_3$ film [17], and R_L is the series resistance which models the resistive contribution of the $SrRuO_3$ lines connecting the device to the contact pads. When a dc voltage is applied to the circuit of fig. 2 the capacitor is an

open circuit, in this way the sum of the parallel and of the series resistor can be estimated. Current versus voltage measurements on $SrRuO_3$ lines reveals a $SrRuO_3$ resistivity of 2.84 Ωμm, in agreement with values reported in [18], and this value can be used to estimate the series resistance so that the parallel resistor can be calculated by subtracting the series resistance from the measured dc resistance.

The impedance of the circuit shown in fig. 2 has the following expression:

$$z(j\omega) = R_L + R / [1+(\omega CR)^2] - j\, \omega C(R)^2 / [1+(\omega CR)^2] \qquad (2).$$

The value of the capacitance can be estimated by equating the measured imaginary part of the impedance to the imaginary part of the right hand side of equation 2. This gives rise to quadratic equation, the root that is inconsistent with the real part of the impedance obtained using the series and parallel resistances as described above is rejected.

This can be repeated at different frequencies and finally the estimated capacitance can be chosen equal to the average of the calculated values. Once that the parameters R, R_L and C have been estimated, their value have been refined by minimizing the quantity:

$$[Re(z)_m - Re(z)_p]^2 + [Im(z)_m - Im(z)_p]^2 \qquad (3)$$

where $Re(z)_m$ is the measured real part of the impedance and $Re(z)_p$ is the real part of the impedance calculated by assuming the lumped element model of fig. 2, similar nomenclature has been used for the imaginary part of the impedance.

4 Results and discussion

As previously stated the $YBa_2Cu_3O_7$ was chosen as the sacrificial layer because it is easy to etch in weak HNO_3 solutions. Furthermore it allows the subsequent epitaxial growth of thin films like $BaTiO_3$, $SrRuO_3$, $SrTiO_3$ and MgO.

Fig. 3 shows a $SrRuO_3/BaTiO_3/SrRuO_3$ u-shape cantilever with a simple beam connected in series, the three-layer were grown on a $YBa_2Cu_3O_7$ sacrificial layer which was removed by undercutting. The $SrRuO_3$ works as an electrode layer for the ferroelectric capacitor and the $BaTiO_3$ is the piezoelectric material.

Alternatively MgO can be chosen as sacrificial layer, however in this case stronger HNO_3 solutions are necessary for its undercut

4.1 X-ray diffraction analysis

X-ray diffraction measurements performed on different thin film stacks grown on $YBa_2Cu_3O_7$ sacrificial layers showed that the $BaTiO_3$ grows with the polar axis perpendicular to the plane of the film on $SrTiO_3$ and on $SrRuO_3$, while it grows with the polar axis parallel to the plane of the film on MgO, as summarized in Table 1. This may be due to the smaller lattice mismatch between the $BaTiO_3$ polar axis and the lattice constant of MgO [8].

In the case of $BaTiO_3$ grown on a MgO film the measured polar lattice parameter of 4.002 Å appears smaller than the bulk value because it is an average value. There are two possible orthogonal orientations when the polar axis is in the plane of the substrate and a non polar axis must also lie in plane [7]. For a 100 nm thick $BaTiO_3$ film sandwiched between two $SrRuO_3$ layers, see Table 1, the polar axis showed an elongation equal to the 0.83% of its length in bulk material, in agreement with observations [12].

When the polar axis is perpendicular to the plane of the film, the polarization can be easily accessed by a parallel plate capacitor, so a three-layer $SrRuO_3/BaTiO_3/SrRuO_3$ parallel plate capacitor grown on the top of a $YBa_2Cu_3O_7$ film works as a 31 device (SBSY device). To improve the interface between the $YBa_2Cu_3O_7$ and the $SrRuO_3$ and to achieve a better undercut of the sacrificial layer, a $SrTiO_3$ buffer layer can be introduced between the sacrificial layer and the bottom electrode [7]. The layer sequence which has to be deposited to produce a 31 device is then: $SrRuO_3/BaTiO_3/SrRuO_3/SrTiO_3/YBa_2Cu_3O_7$ (SBSSY device).

When the polar axis is parallel to the surface of the film, the polarization can be accessed by using an interdigitated capacitor. In this case a $SrRuO_3/BaTiO_3/MgO/YBa_2Cu_3O_7$ (SBMY device) stack can be used. The MgO layer changes the growth orientation of the $BaTiO_3$ (and it is not used as sacrificial layer in this sequence), the consequence is that the polar axis will be parallel to the surface of the film. Again to achieve a more efficient undercut a $SrTiO_3$ buffer layer can be introduced between the MgO and the $YBa_2Cu_3O_7$ [7]. So the layer sequence to use in the case of a 33 device is: $SrRuO_3/BaTiO_3/MgO/SrTiO_3/ YBa_2Cu_3O_7$ (SBMSY device). If an MgO sacrificial layer is used the sequence becomes $SrRuO_3/BaTiO_3/MgO$ (SBM device).

In the case of a MgO sacrificial layer, the stacks to use as 31 devices are $SrRuO_3/BaTiO_3/SrRuO_3/MgO$ (SBSM device) and $SrRuO_3/BaTiO_3/SrRuO_3/SrTiO_3/MgO$ (SBSSM device). For the SBSSM device the use of the $SrTiO_3$ layer allows the growth of $BaTiO_3$ with the polar axis out of plane all over the sample after the patterning and the milling of the $SrRuO_3$ bottom electrode.

The use of the MgO sacrificial layer presents the advantage of dealing with a simple tri-layer, however the undercut of the MgO requires a wet etching of several hours in 20% HNO_3. When

the $YBa_2Cu_3O_7$ is used, a wet etch of few minutes in 0.1% HNO_3 is necessary to suspend the structures.

4.2 Impedance measurements and AFM investigation

Impedance measurements showed that $SrRuO_3$(100 nm)/$BaTiO_3$(400 nm)/$SrRuO_3$(150 nm) and $SrRuO_3$(100)/$BaTiO_3$(300 nm)/MgO(60 nm) structures grown on $SrTiO_3$ substrates have capacitive behavior when the $BaTiO_3$ is deposited in oxygen flow at a pressure equal or lower than 8 Pa. This is shown by the value of the impedance phase. Fig. 4 shows the modulus and the phase of the impedance for a $SrRuO_3$/$BaTiO_3$/ $SrRuO_3$ device. Its phase varies between -85 and -82 in the frequency range 40Hz-40 kHz revealing a clear capacitive behavior. When the $BaTiO_3$ was deposited in oxygen flow at a pressure of 20 Pa these structures exhibited resistive behavior [7].

With the introduction of an oxide sacrificial layer under the multi-layer capacitive structures the electrical properties of the $BaTiO_3$ change.

For $YBa_2Cu_3O_7$ used as sacrificial layers, SBSSY 31 mode and SBMSY 33 mode structures have been investigated.

The $BaTiO_3$ films were grown at pressures of 8 Pa. These devices presented poor capacitive behavior. Fig.5 shows the impedance measurement on a SBSSY 31 device with the $BaTiO_3$ layer deposited at a pressure of 8 Pa. In this case the impedance is mainly resistive, around 20 kHz some capacitive effect starts to be visible, at 50 kHz the impedance phase is around -23 . Our impedance analyzer allows a minimum measurement frequency of 40Hz, at which frequency the

phase of the impedance is equal to -0.1 so the impedance can be considered as pure resistive and the parallel and the series resistances can be calculated.

The parallel resistance is estimated equal to 1.4 KΩ resulting in a resistance area (RA) product of $44.1*10^5$ Ωμm^2. The calculated series resistance has a value of 1.086 KΩ and the estimated capacitance is equal to 1.98 nF resulting in a capacitance per unit area (C/A) of $6.28*10^{-13}$ F/μm^2. Fig. 5 also shows a fit to the data obtained using the lumped element model, illustrating the good agreement between the model and the measured data. This device shows poor capacitive behavior to the extent that the low value of the parallel resistance dominates the parallel capacitor. Despite this, X-ray measurements on stacks grown on $YBa_2Cu_3O_7$ sacrificial layers, revealed the presence of a crystal structure in the $BaTiO_3$ films.

Studies on the pulsed laser deposition of $YBa_2Cu_3O_7$ films reported the presence of different types of particulates on their surface [19]. It is likely that such particulates degrade the quality of the layers deposited on their surface, by creating resistive paths through the capacitive structures which might be responsible for the low value of the RA product.

In order to investigate this, an Atomic Force Microscope was used to examine the surface of the deposited $YBa_2Cu_3O_7$ films. Fig. 6a shows an AFM scan on the surface of a 150 nm $YBa_2Cu_3O_7$ layer, on whose surface it is possible to see an outgrowth with a height comparable to the film thickness, despites the relatively low deposition temperature. Such outgrowths are also present after the deposition of a 100 nm $SrTiO_3$ layer as shown in, fig. 6b. The effect of such outgrowths on the upper layers can be reduced using a thicker $SrTiO_3$ layer. Fig. 6c shows an AFM scan on a $SrTiO_3$(500 nm)/ $YBa_2Cu_3O_7$(400 nm) bi-layer which confirms that the particulates present on the surface of the film are fewer in number and generally smaller.

Fig. 7 reports the impedance measurements of a SBSSY device with a 1 μm thick $SrTiO_3$ film on the $YBa_2Cu_3O_7$ sacrificial layer. The oxygen pressure during deposition of the $BaTiO_3$ was equal to 8 Pa. Also in this case the impedance is not fully capacitive, at 40 Hz the impedance phase is equal to -0.5 , again at such frequency the impedance is considered as purely resistive and so the parallel and the series resistances can be estimated. The series resistance is equal to 1.086 KΩ, the parallel resistance has a value of 31.78 KΩ resulting in a RA product of $19.54*10^7$ $\Omega\mu m^2$ and the capacitance is equal to 480 pF, giving a C/A of $7.8*10^{-14}$ $F/\mu m^2$.

The lines in figs. 7 represent the modulus and the phase for the impedance of the lumped element model, the points are the measured values. The impedance modulus of the lumped element model agrees quite well with the measured data while an error of 8% is present in the value of the impedance phase over 20 kHz.

The introduction of a thicker $SrTiO_3$ buffer layer reduces the parasitic shunting conductance and so the losses which are present in the $BaTiO_3$ film due to the outgrowths on the surface of the $YBa_2Cu_3O_7$ sacrificial layer. This is illustrated by the higher value of the RA product, however the quality of these devices is still not satisfactory especially at low frequencies where the resistive part of the impedance dominates.

In the case of capacitors grown directly on the substrate it has been demonstrated that the reduction of the $BaTiO_3$ deposition pressure reduces the parasitic shunting conductance and so losses present in the film [7]. When a $YBa_2Cu_3O_7$ sacrificial layer is used a further reduction of the $BaTiO_3$ deposition pressure is not possible as there would be dissociation of the sacrificial layer at the $BaTiO_3$ deposition temperature [20].

Another solution is to use an MgO sacrificial layer, as this material can still be etched in HNO_3 although a high acid concentration and longer etching time are necessary. The advantage of the MgO sacrificial layer is that it does not dissociate at low pressures at the $BaTiO_3$ deposition temperature.

Fig. 8 shows the impedance measurement on a SBSSM device. Assuming for this device the model of fig. 2, the resistance of the lines R_L is 1.17 KΩ, the parallel resistor R is equal to 1.966 MΩ resulting in a RA product of $61.93*10^8$ Ωμm^2. The capacitance is equal to 95.66 pF, giving a C/A of $3.04*10^{-14}$ F/μm^2. The plots show a good agreement between the model and the measured data.

There is a difference of one order of magnitude between the RA product of this device and that one of the device using a 1μm thick $SrTiO_3$ buffer layer on a $YBa_2Cu_3O_7$ sacrificial layer. Compared to that case, this high value of the RA product makes the capacitive part of the impedance dominate at much lower frequencies. At 5.5 kHz the phase of the total impedance is equal to -80 , the capacitive part of the impedance is roughly 7 times smaller than the parallel resistance and 250 times bigger than the series resistance, so over 5.5 kHz the device can be approximated as a pure capacitor.

If the $BaTiO_3$ deposition pressure is further reduced to 0.013 Pa the losses are eliminated also at low frequency, this is shown in fig. 9, and an impedance phase of 88 is already present at 50Hz. Due to the high value of the impedance phase at low frequencies, the parallel resistor can be approximated as an open circuit and the equivalent model of the device is given by the resistor R_L in series with the capacitor C. For this device the series resistance was estimated equal to 1.086 KΩ while the capacitance is equal to 55.57 pF resulting in a C/A of $1.76*10^{-14}$ F/μm^2. By

using these values in the lumped element model good agreement is obtained with the measured data, fig. 9. This demonstrates that a reduction of the $BaTiO_3$ deposition pressure reduces the parasitic shunting conductance and so the resistive losses present in the film. Furthermore in this case the approximation of the parallel resistor with an open circuit works quite well and the behavior of the device can be approximated as purely capacitive.

The reduction of the $BaTiO_3$ deposition pressure also produces a reduction in the value of the parallel capacitance. Figs. 8 and 9 report the impedance measurements of two devices with the same faced area and the same $BaTiO_3$ thickness. For a $BaTiO_3$ deposition pressure of 8 Pa a C/A of $3.04*10^{-14}$ F/μm^2 was measured while for a $BaTiO_3$ deposition pressure of 0.013 Pa the C/A was reduced to $1.76*10^{-14}$ F/μm^2. It was reported that in $SrTiO_3/BaTiO_3$ systems grown by Pulsed Laser Deposition the dielectric constant increases when the oxygen deposition pressure increases [21]. If the oxygen pressure during the growth of the thin films is low it is more favorable to form oxygen vacancies in the oxide films during the process which results in a decrease of the dielectric constant [21].

The layer sequences, the RA products, the C/A and the $BaTiO_3$ deposition pressures for the investigated devices are summarized in table 2.

4.3 Hysteresis measurements

The disadvantage of extremely low $BaTiO_3$ deposition pressures is the degradation of the hysteresis loop of the ferroelectric capacitors. Fig. 10a represents the hysteresis loop of a $SrRuO_3/BaTiO_3/SrRuO_3$ capacitor grown on the $SrTiO_3$ substrate at a pressure of 8 Pa, in this case the residual polarization is equal to 5.3 μC/cm^2. Fig. 10b shows the hysteresis loop of a SBSSM device containing a $BaTiO_3$ at a pressure of 8 Pa, the residual polarization is equal to 2.5

$\mu C/cm^2$. Finally fig. 10c shows the hysteresis loop of a SBSM device having a $BaTiO_3$ film grown at a pressure of 0.013 Pa. In this case the hysteresis behavior is not clear and the loop seems to be degraded into a double loop.

The presence of defects in the $BaTiO_3$ film can produce a distorted loop as that one reported in fig. 10c [22]. Oxygen vacancies produce a lower dielectric constant in $BaTiO_3$ films grown at low pressure, so we believe that the degradation of the hysteresis loops arises from defects due to oxygen deficiency in the $BaTiO_3$ film.

4.4 Discussion

The performances of $BaTiO_3$ based ferroelectrics capacitors grown on MgO and $YBa_2Cu_3O_7$ sacrificial layers have been assessed. These sacrificial layers allow the epitaxial growth of thin film stacks containing $BaTiO_3$, $SrRuO_3$ and $SrTiO_3$.

In both cases in order to produce a capacitive structure the oxygen pressure used for deposition of the $BaTiO_3$ should be equal to or lower than 8 Pa.

For PLD deposition depending on the surface mobility of the atoms, the growth of the film may be accompanied by the formation of stacking faults and amorphous and void like grain boundaries [23]. The surface mobility of the atoms is influenced by the deposition pressure, the substrate temperature and the laser energy.

Our investigations show that a reduction of the $BaTiO_3$ deposition pressure reduces the losses present in the fabricated capacitors, this happens either in the case of capacitors grown on the substrate or on the sacrificial layer. Higher deposition pressures imply a larger number of

collisions in the path between the material target and the substrate. The energy lost in the ablation path produces a lower mobility of the atomic species on the substrate [19].

In the case of multi-layers grown on the top of $SrTiO_3$(250 nm)/$YBa_2Cu_3O_7$(500 nm) bi-layers, the presence of outgrowths on the surface of the $YBa_2Cu_3O_7$ sacrificial layer, produces a low value of the parallel resistance which dominates the parallel capacitance.

With the introduction of a thicker $SrTiO_3$ buffer layer the effect of the $YBa_2Cu_3O_7$ outgrowths on the fabricated capacitor is reduced and this is testified by an increase of the RA product.

However a further reduction of the film losses which correspond to an increase of the RA product and to a decrease of the parasitic shunting conductance is desirable. To reduce the losses present in the $BaTiO_3$ film its deposition pressure can be reduced, however for multi-layers containing $YBa_2Cu_3O_7$ the minimum $BaTiO_3$ deposition pressure is limited by the dissociation of the sacrificial layer.

The structures grown on the MgO sacrificial layer show a value of the resistance area product which is at least one order of magnitude bigger than that one of the devices using the $YBa_2Cu_3O_7$ sacrificial layer. Furthermore the RA product increases with the reduction of the $BaTiO_3$ deposition pressure this produce structures approaching the behavior of a pure capacitor. However with the reduction of the deposition pressure the value of the capacitance per unit area decreases and the quality of the hysteresis loop downgrades. This may be due to the oxygen vacancies present in $BaTiO_3$ grown at low pressures.

To increase the mobility of the atomic species on the substrate, a higher $BaTiO_3$ deposition temperature rather than a low deposition pressure can be used. Stacks containing a $BaTiO_3$ layer grown at temperatures of 850 °C and at a pressure of 8 Pa, show the presence of holes on the top

surface of the stack which can be due to thermal stresses produced during the cooling down of the multi-layers. Furthermore some layers peel off during the wirebonding of the pads of the capacitors, necessary for the electrical characterization of the devices.

Another parameter which can be used to increase the mobility on the substrate of the incoming atoms is the laser energy, however the deposition energy is very near to the maximum achievable with our apparatus.

5 Conclusions

All oxide multi-layer structures containing $BaTiO_3$ can find applications as MEMS devices in the field of energy harvesting or as components of sensors and actuators. Layers sequences like $SrRuO_3/BaTiO_3/SrRuO_3/SrTiO_3/YBa_2Cu_3O_7$ (SBSSY device), $SrRuO_3/BaTiO_3/SrRuO_3/SrTiO_3/MgO$ (SBSSM device), $SrRuO_3/BaTiO_3/MgO/SrTiO_3/YBa_2Cu_3O_7$ (SBMSY device) and $SrRuO_3/BaTiO_3/SrTiO_3/MgO$(SBSM device) allow the use of both the 31 and the 33 piezoelectric modes.

The $YBa_2Cu_3O_7$ is easily etched in weak acids like 0.1% HNO_3 however the structures grown on top do not behave as pure capacitors but present losses.

The stacks grown on the MgO sacrificial layer show a value of the resistance area product which is at least one order of magnitude bigger than that one of the devices using the $YBa_2Cu_3O_7$ sacrificial layer. Furthermore the RA product increases with the reduction of the $BaTiO_3$ deposition pressure but the quality of the hysteresis loop downgrades.

A good compromise is reached for the $BaTiO_3$ deposition pressure of 8 Pa.

Future developments for these kind of structures consist in the reduction of the resistive losses for the stacks containing $YBa_2Cu_3O_7$ and in the recovery of the capacitive behavior at low frequencies.

For the stacks using the MgO sacrificial layer, and for $BaTiO_3$ growth pressures equal to 8 Pa, a reduction of the resistive losses below 1 kHz it is necessary. Alternatively an improving of the hysteresis loop can be reached for the multi-layers containing $BaTiO_3$ grown at pressures below 8 Pa.

Acknowledgements

This research has been funded by the UK EPSRC under EP/E026494/1 and by The University of Birmingham.

References

1 Y. B. Jeon, R. Sood, J. H. Jeong, S. G. Kim, Sensor Actuat. A-Phys. 122 (2000) 16

2 J. W. Choi, Y. Jeon, J. H. Jeong, R. Sood, S. G. Kim, J. Electroceram. 17 (2006) 543

3 Q. Q. Zhang, S. J. Gross, S. Tadigadapa, T. N. Jackson, F. T. Djuth, S. T. McKinstry, Sensor Actuat. A-Phys. 105 (2003) 91

4 F. F. C. Duval, S. A. Wilson, G. Ensell, N. M. P. Evanno, M. G. Cain, R. W. Whatmore, Sensor Actuat. A-Phys. 133 (2007) 35

5 F. F. C. Duval, R. A. Dorey, R. W. Wright, Z Huang, R. W. Whatmore, IEEE Trans. Ultrason., Ferroelectr., Freq. Control 51(2004) 1255

6 N. Setter, D. Damjanovic, L. Eng, G. Fox, S. Gevorgian, S. Hong, A Kingon, H. Kohlstedt, N. Y. Park, G. B. Stephenson, I. Stolitchnov, A. K. Taganstev, D. V. Taylor, T. Yamada, S Streiffer, J. Appl. Phys. 100 (2006) 051606-1

7 G. Vasta, T. J. Jackson, J. Bowen, E. Tarte, New multilayer architecture for piezoelectric $BaTiO_3$ cantilever systems**,** MRS Proc. 1325 (2011) e08-05

8 F. X. Wang, W. Li, F. Lu, H. Hu, K. M. Wang, Z. G. Liu, Y. Zhu, Nucl. Instr. Meth. Phys. Res. B 191 (2002) 778

9 K. Sato, M. Takahashi, N. Matsunami, Y. Takai, Supercond. Sci. Tech. 9 (1996) A156

10 D. H. Kim, H. S. Kwok (1995), Appl. Phys. Lett. 67 (1995) 1803

11 Y. Yang, Z. Wang , J. F. Li, D. Viehland, J. Nanomater. 2010 (2010) 756319

12 K. J. Choi, M. Biegalski, Y. L. Li, A. Sharan, J. Schubert, R. Uecker, P. Reiche, Y. B. Chen, X. Q. Pan, V. Gopalan, L. Q. Chen, D. G. Schlom, C. B. Eom, Science 306 (2004) 1005

13 H. Sato, F. J. G. Roesthuis, A. H. Sonnenberg, A. J. H. M.Rijnders, H. Rogalla, D. H. A. Blank, Supercond. Sci. Tech. 13 (2000) 522

14 H. J. H. Smilde, H. Hilgenkamp, G. J. Gerritsma, D. H. A. Blank, H. Rogalla, IEEE Trans Appl. Supercond. 11 (2001) 501

15 L. Pellegrino, M. Biasotti, E. Bellingeri, C. Bernini, A. S. Siri, D. Marre`, Adv. Mater. 21 (2009) 2377

16 D. Berlincourt, H. Jaffe, Phys. Rev. 111 (1958) 143

17 E. J. Abram, D. C. Sinclair, A. R. West, J. of Electroceram. 10 (2003) 165

18 X. D. Wu, S. R. Foltyn, R. C. Dye, Y. Coulter, R. E. Muenchausen, Appl. Phys. Lett. 62 (1993) 2434

19 S. Proyer, E. Stangl, M. Borz, B. Hellebrand, D. Bauerle, Physica C 257 (1996) 1

20 R. Wordenweber, Supercond. Sci. Tech. 12 (1999) R86

21 B. R. Kim, T. U. Kim, W. J. Lee, J. H. Moon, B. T. Lee, H. S. Kim, J. H. Kim, Thin Solid Films 515 (2007) 6438

22 M. E. Lines, A. M. Glass, Principles and applications of ferroelectrics and related materials, Clarendon Press Oxford 1977

23 D. Su, T. Yamada, R. Gysel, A. K. Tagantsev, P. Murat N. Setter, N Jiang, J. Mater. Res. 26 (2011) 770

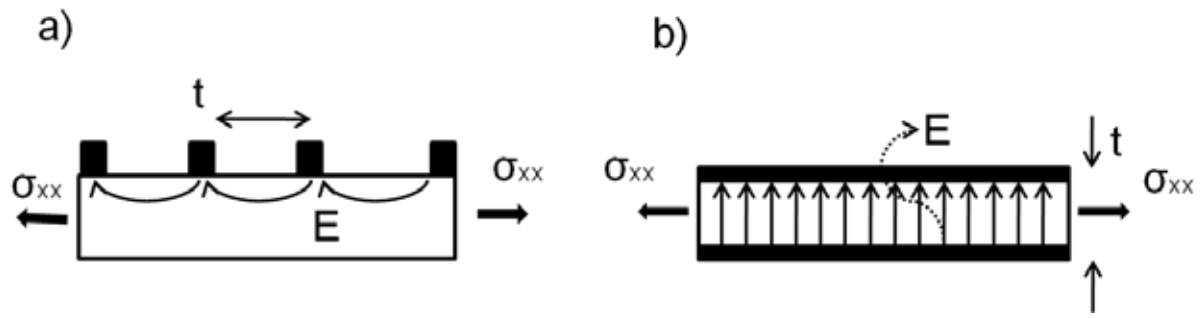

Fig. 1 a) 33 piezoelectric conversion mode, σ_{xx} is the applied external stress, t is the spacing between the fingers of the electrode and E is the electric field sensed by the electrodes. b) 31 piezoelectric conversion mode, σ_{xx} is the applied external stress, t is the spacing between the top and the bottom electrode and E is the electric field sensed by the electrodes.

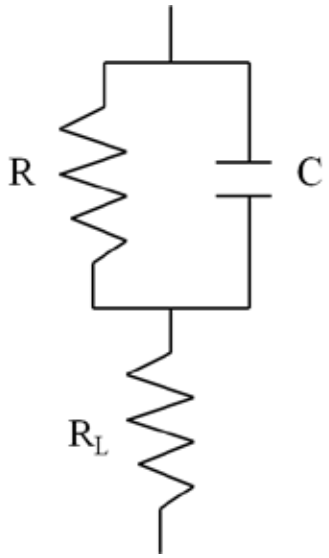

Fig. 2 Equivalent model for $SrRuO_3/BaTiO_3/SrRuO_3$ structures showing resistive impedance at low frequency and capacitive impedance at high frequency. The resistor R_L models the resistance of the lines, the resistor R in parallel with the capacitor C models the $BaTiO_3$ film.

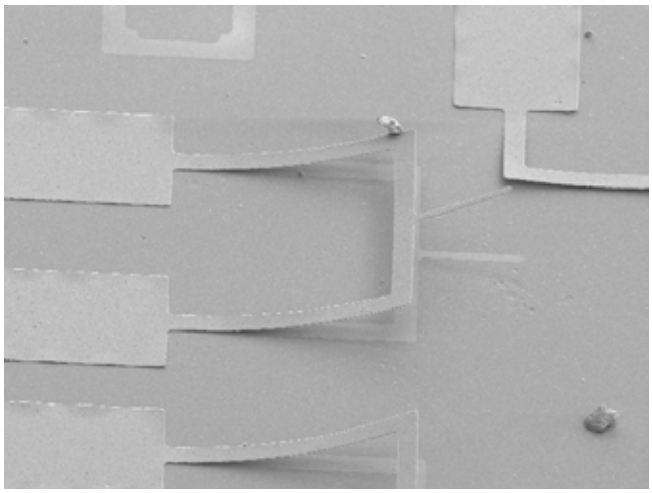

Fig. 3 $SrRuO_3/BaTiO_3/SrRuO_3$ u-shape cantilever with a simple beam connected in series. The total length of the structure is equal to 260 μm. The tri-layer was grown on a $YBa_2Cu_3O_7$ sacrificial layer.

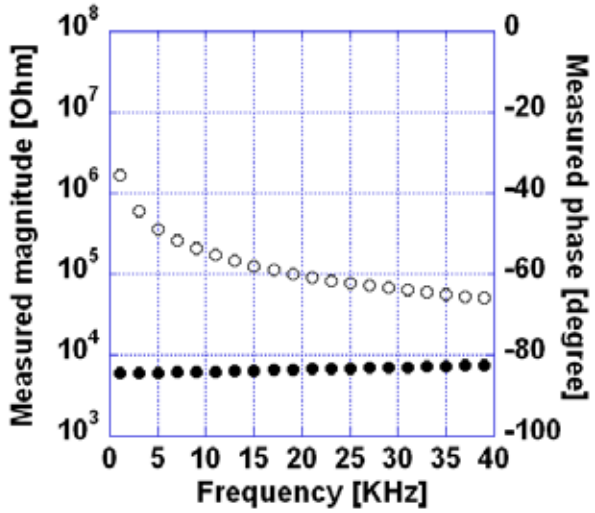

Fig. 4 Impedance measurements on a 105 μm x 30 μm $SrRuO_3$(100 nm)/$BaTiO_3$(400 nm)/$SrRuO_3$(150 nm) parallel plate capacitor grown on a (001) oriented $SrTiO_3$ substrate. The $BaTiO_3$ was grown at 780 C at a pressure of 0.06 Torr O_2. Impedance measurements were performed with an input signal amplitude of 1 V. The open circles (○○) show the modulus of the measured impedance, while the full circles (●●) show the measured impedance phase of the structure.

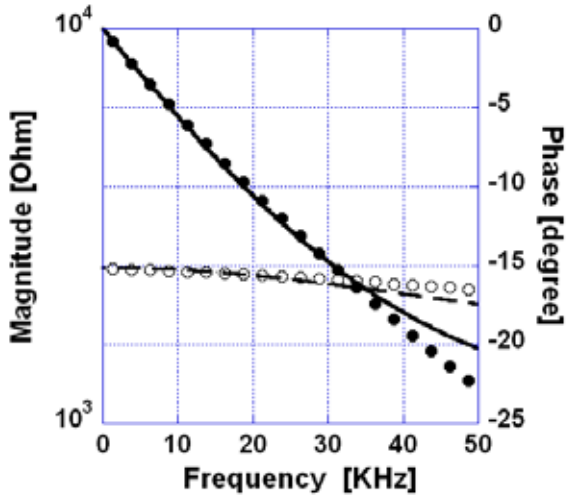

Fig. 5 Impedance measurements on a 105 μm x 30 μm $SrRuO_3$(100 nm)/$BaTiO_3$(300 nm)/$SrRuO_3$(150 nm) parallel plate capacitor grown on a $SrTiO_3$(250 nm)/$YBa_2Cu_3O_7$(500 nm) bi-layer. The $BaTiO_3$ was grown at 780 C at a pressure of 0.06 Torr O_2. Impedance measurements were performed with an input signal amplitude of 1 V. The dashed line (- -) represents the modulus of the impedance for the lumped element model, while the open circles (○○) show the modulus of the measured impedance. The continuous black line (—) line represents the impedance phase of the circuit used to model the device, while the full circles (●●) indicate the measured impedance phase of the structure.

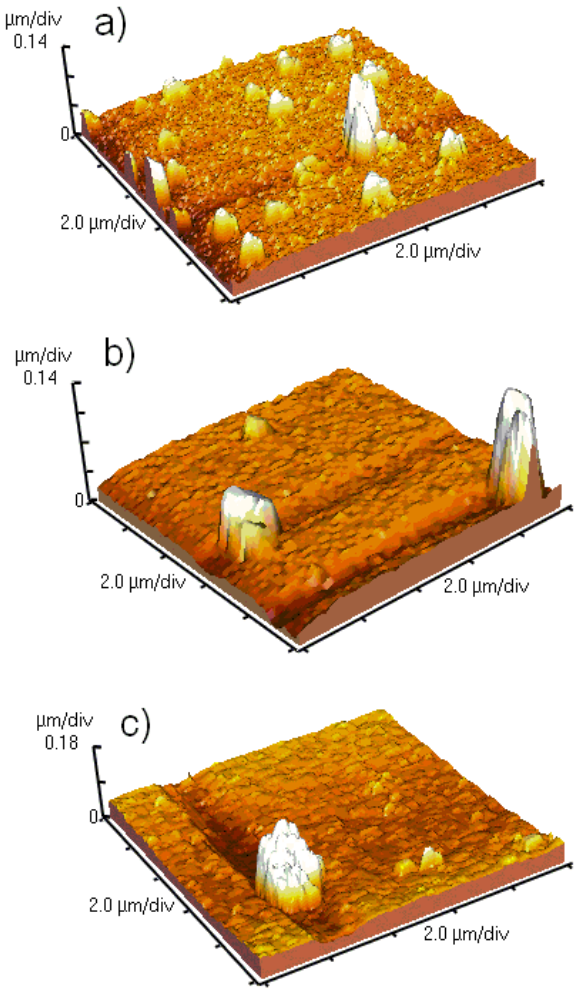

Fig. 6 AFM scan of a 10 µm x 10 µm area of: a) 150 nm $YBa_2Cu_3O_7$ film, b) $SrTiO_3$(100 nm)/ $YBa_2Cu_3O_7$(150 nm) bi-layer, c) /$SrTiO_3$(500 nm)/ $YBa_2Cu_3O_7$(400 nm) bi-layer.

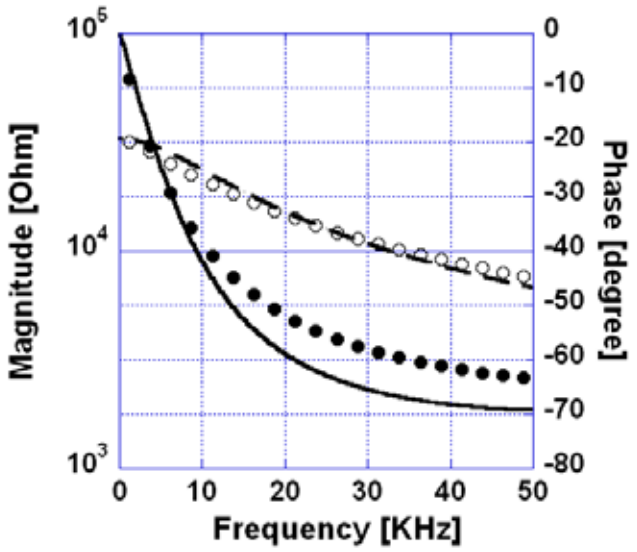

Fig. 7 Impedance measurements of a 205 μm x 30 μm $SrRuO_3$(100 nm)/$BaTiO_3$(300 nm)/$SrRuO_3$(150 nm) parallel plate capacitor grown on a $SrTiO_3$(1 μm)/$YBa_2Cu_3O_7$(500 nm) bi-layer. The $BaTiO_3$ was grown at 780 C at a pressure of 0.06 Torr O2. Impedance measurements were performed with an input signal amplitude of 1 V. The dashed line (- -) shows the modulus of the impedance for the lumped element model, while the open circles (○○) show the modulus of the measured impedance. The continuous black line (—) line shows the impedance phase of the circuit used to model the device, while the full circles (●●) indicate the measured impedance phase of the structure.

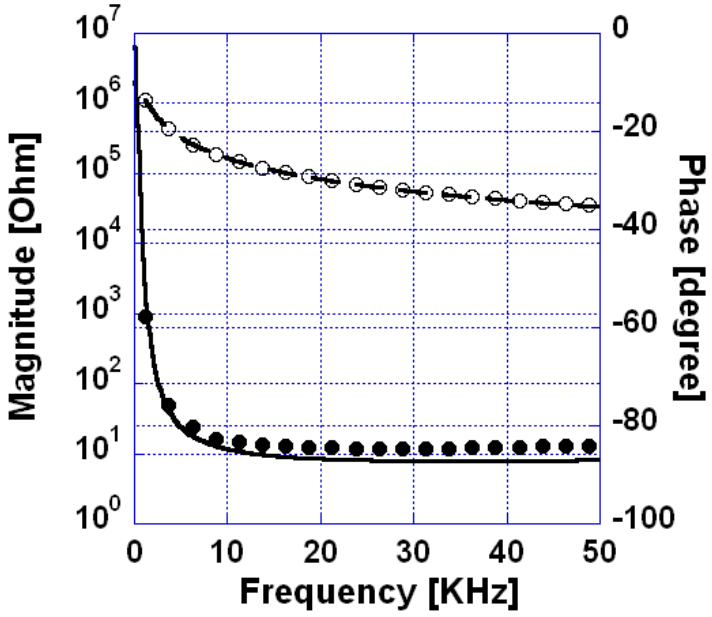

Fig. 8 Impedance measurement of a 105 μm x 30 μm $SrRuO_3$(100 nm)/$BaTiO_3$(300 nm)/$SrRuO_3$(150 nm) parallel plate capacitor grown on a $SrTiO_3$(250 nm)/MgO(400 nm) bi-layer. The $BaTiO_3$ was grown at 780 C at a pressure of 0.06 Torr O2. Impedance measurements were performed with an input signal amplitude of 1 V. The dashed line (- -) shows the modulus of the impedance for the lumped element model, while the open circles (○○) show the modulus of the measured impedance. The continuous black line (—) line shows the impedance phase of the circuit used to model the device, while the full circles (●●) indicate the measured impedance phase of the structure.

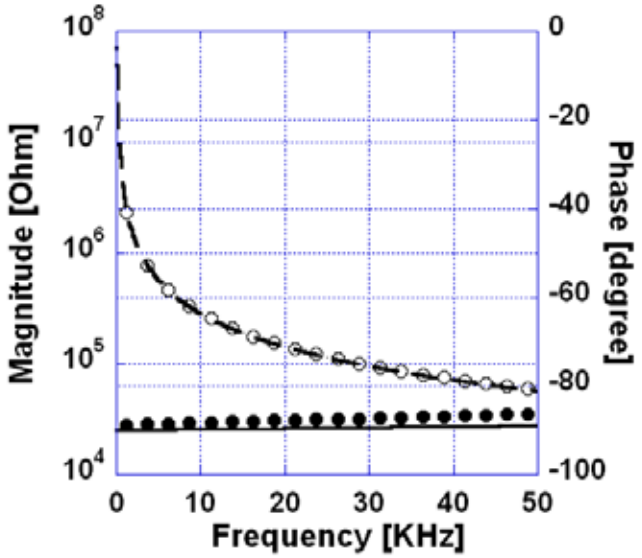

Fig. 9 Impedance measurement of a 105 μm x 30 μm $SrRuO_3$(100 nm)/$BaTiO_3$(300 nm)/$SrRuO_3$(150 nm) parallel plate capacitor grown on a MgO(400 nm) sacrificial layer. The $BaTiO_3$ was grown at 780 C at a pressure of 0.1 mTorr O2. Impedance measurements were performed with an input signal amplitude of 1 V. The dashed line (- -) shows the modulus of the impedance for the lumped element model, while the open circles (○○) show the modulus of the measured impedance. The continuous black line (—) line shows the impedance phase of the circuit used to model the device, while the full circles (●●) indicate the measured impedance phase of the structure.

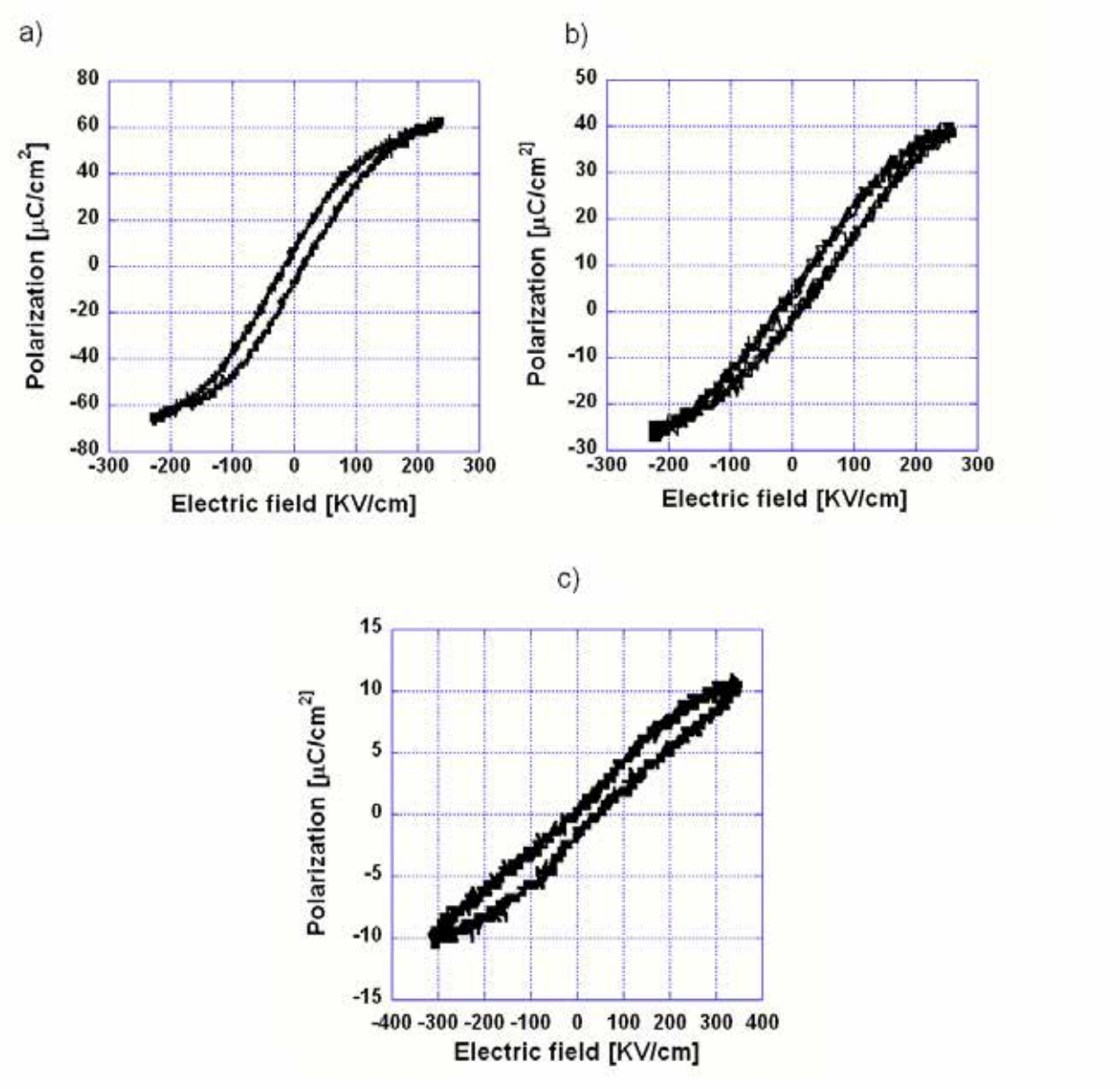

Fig. 10 a) Hysteresis loop measurements on a $SrRuO_3$(100 nm)/$BaTiO_3$(400 nm)/$SrRuO_3$(150 nm) parallel plate capacitor directly deposited on the $SrTiO_3$ substrate. The $BaTiO_3$ film was grown at a pressure of 0.06 Torr. b) Hysteresis loop measurements on a $SrRuO_3$(100 nm)/$BaTiO_3$(300 nm)/$SrRuO_3$(150 nm) parallel plate capacitor deposited directly on a $SrTiO_3$(250nm)/MgO(400 nm) bi-layer. The $BaTiO_3$ film was grown at a pressure of 0.06 Torr. c) Hysteresis loop measurements on a $SrRuO_3$(100 nm)/$BaTiO_3$(300 nm)/$SrRuO_3$(150 nm) parallel plate capacitor deposited on a 400 nm thick MgO layer, the $BaTiO_3$ film was grown at a pressure of 0.1 mTorr.

.

Material [top down layer sequence]	**In plane a axis measured [Å] (bulk [Å])**	**In place b axis measured [Å] (bulk [Å])**	**Out of plane axis measured [Å] (bulk [Å])**
$BaTiO_3$ [$SrRuO_3$(50nm)/$BaTiO_3$(100nm)/ $SrRuO_3$(350nm)/$YBa_2Cu_3O_7$(400nm)]	3.951 (3.992)	3.951 (3.992)	4.069 (4.036)
$BaTiO_3$ [$BaTiO_3$(500nm)/MgO(60nm)/ $YBa_2Cu_3O_7$(400nm)]	4.002 (3.992)	4.002 (3.992)	3.997 (4.036)
$BaTiO_3$ [$BaTiO_3$(126nm)/$SrTiO_3$(500nm)/ $YBa_2Cu_3O_7$(400nm)]	3.996 (3.992)	3.996 (3.992)	4.015 (4.036)

Table 1: $BaTiO_3$ film lattice parameters on different layer sequences. Bulk parameters are provided for comparison.

Device (fig)	**Top down layer sequence**	**$BaTiO_3$ deposition pressure [Pa]**	**RA product [$\Omega\mu m^2$]**	**C/A ratio [$F/\mu m^2$]**
SBSSY (fig. 5)	$SrRuO_3$(100nm)/$BaTiO_3$(300nm)/ $SrRuO_3$(150nm)/$SrTiO_3$(250nm)/ $YBa_2Cu_3O_7$(500nm)	8	$44.1*10^5$	$6.28*10^{-13}$
SBSSY (fig. 7)	$SrRuO_3$(100nm)/$BaTiO_3$(300nm)/ $SrRuO_3$(150nm)/$SrTiO_3$(1000nm)/ $YBa_2Cu_3O_7$(500nm)	8	$19.54*10^7$	$7.8*10^{-14}$
SBSSM (fig. 8)	$SrRuO_3$(100nm)/$BaTiO_3$(300nm)/ $SrRuO_3$(150nm)/ $SrTiO_3$(250nm)/ MgO(400 nm)	8	$61.93*10^8$	$3.04*10^{-14}$
SBSM (fig. 9)	$SrRuO_3$(100nm)/$BaTiO_3$(300nm)/ $SrRuO_3$(150nm)/MgO(400 nm)	0.013	$\approx \infty$	$1.76*10^{-14}$

Table 2: Top down layer sequences, $BaTiO_3$ deposition pressure, RA product and C/A ratio of the structures under investigation, the figure numbers showing the impedance measured of each device are reported.